ACS APPLIED MATERIALS & INTERFACES

Research Article

www.acsami.org

Tunable and Robust Phosphite-Derived Surface Film to Protect Lithium-Rich Cathodes in Lithium-Ion Batteries

Jung-Gu Han,[†] Sung Jun Lee,[†] Jaegi Lee,[†] Jeom-Soo Kim,[‡] Kyu Tae Lee,*[,§] and Nam-Soon Choi*[,†]

[†]School of Energy and Chemical Engineering, Ulsan National Institute of Science and Technology (UNIST), 100 Banyeon-ri, Eonyang-eup, Ulju-gun, Ulsan 689-798, South Korea

[‡]Department of Chemical Engineering, Dong-A University, Busan 604-714, South Korea

[§]School of Chemical and Biological Engineering, Seoul National University, 599 Gwanangno, Gwanak-gu, Seoul 151-744, South Korea

Supporting Information

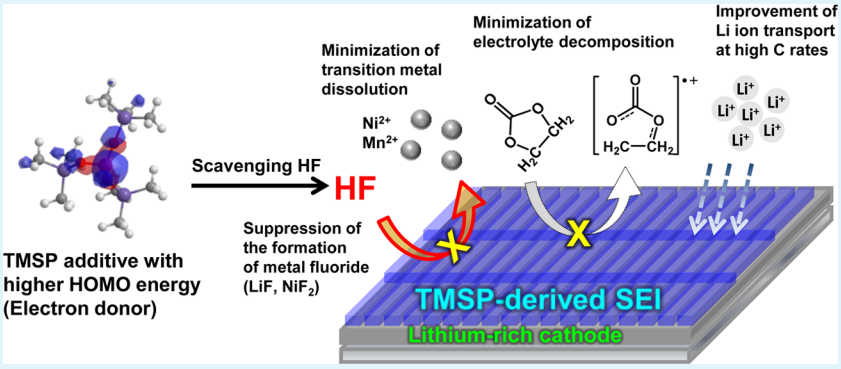

ABSTRACT: A thin, uniform, and highly stable protective layer tailored using tris(trimethylsilyl) phosphite (TMSP) with a high tendency to donate electrons is formed on the Li-rich layered cathode, $Li_{1.17}Ni_{0.17}Mn_{0.5}Co_{0.17}O_2$. This approach inhibits severe electrolyte decomposition at high operating voltages during cycling and dramatically improves the interfacial stability of the cathode. The TMSP additive in the $LiPF_6$-based electrolyte is found to preferentially eliminate HF, which promotes the dissolution of metal ions from the cathode. Our investigation revealed that the TMSP-derived surface layer can overcome the significant capacity fading of the Li-rich cathode by structural instability ascribed to an irreversible phase transformation from layered to spinel-like structures. Moreover, the superior rate capability of the Li-rich cathode is achieved because the TMSP-originated surface layer allows facile charge transport at high C rates for the lithiation process.

KEYWORDS: *electrolyte additive, tris(trimethylsilyl) phosphite, solid electrolyte interphase, lithium-rich layered cathode, lithium-ion battery*

1. INTRODUCTION

Lithium-ion batteries (LIBs) are one of the most promising energy storage technologies because of their high voltage, energy density, and cost-effectiveness.[1−5] Although LIBs have been successfully commercialized, the energy density of lithium-ion cells needs to be improved to satisfy the needs of high power and/or capacity applications such as power tools, electric vehicles (EVs), or renewable energies.[6−9] The energy density of conventional LIBs, with cathodes operating at 3.3−3.9 V, such as $LiCoO_2$ (∼140 mAh g^{-1}) and $LiFePO_4$ (∼160 mAh g^{-1}), is limited. To achieve a LIB energy density greater than 250 Wh kg^{-1}, many research groups have worked hard to increase the voltage and capacity of cathode materials such as $LiNi_{0.5}Mn_{1.5}O_4$ (LNMO)[10,11] and Li-rich cathodes[12,13] with chemical compositions of $xLi_2MnO_3{\cdot}(1-x)LiMO_2$. Li-rich cathodes are the most promising because they have a reasonably high operating voltage and a high reversible capacity, which can exceed 200 mAh g^{-1}.[14−16] Although Li-rich cathode materials can achieve a high energy density, their practical application to LIBs is still quite challenging because Li-rich layered cathodes have a large irreversible capacity due to the Li_2O formed by Li_2MnO_3 activation in the initial cycle and severe electrolyte decomposition at high votlages and the structural instability via irreversible phase transformation.[17−19] The amount of Li_2MnO_3 activated is strongly affected by the cell operating voltage.[20,21] Although the reversible capacity of Li-rich cathodes can be improved by Li_2MnO_3 activation at high voltages, it is important to determine the proper operating voltage because Li_2MnO_3 can help to maintain stable cathode structures.[22] Li-rich cathodes can also undergo irreversible phase transformation from layered to spinel-like structures after prolonged cycling.[23−28] This phase transformation occurs as

Received: February 26, 2015
Accepted: March 30, 2015
Published: March 30, 2015

DOI: 10.1021/acsami.5b01770
ACS Appl. Mater. Interfaces 2015, 7, 8319−8329

transition metal ions in the transition metal layer move into the Li layer. This causes capacity fading because transition metal ions in the Li layer disturb the lithiation or delithiation process, which proceeds gradually from the surface to the bulk of the cathode as cycling progresses. In addition, severe oxidative decomposition of the electrolyte beyond the upper voltage limit (around 4.3 V versus Li/Li^+) of conventional $LiPF_6$-based electrolytes inevitably occurs, because Li-rich cathodes operate at voltages above 4.4 V versus Li/Li^+.[29,30] This causes the formation of a resistive and unstable surface film of inorganic lithium salts and organic carbonates on the cathode. As a result, high-voltage Li-rich cathodes with conventional electrolytes have a large irreversible capacity and low Coulombic efficiency.[31,32] To alleviate the oxidative decomposition of electrolytes on high-voltage cathodes, Al_2O_3,[33] ZrO_2,[34] AlF_3,[35] CaF_2,[36] polyaniline,[37] and reduced graphene oxide/$AlPO_4$ hybrid materials[38] have been used as protective coatings for the cathode. Functional additives are efficient and economic materials, which form a protective layer on the cathode and improve the interfacial stability of Li-rich cathodes by preventing electrolyte decomposition in highly oxidizing environments.[39] In recent years, many studies have reported that the electrochemical performance of Li-ion cells is improved by using electrolyte additives that can suppress unwanted electrolyte decomposition via the formation of a protective layer on the cathode surface.[39,40] For example, oxidative compounds, which oxidize quicker than carbonate-based solvents, form a stable solid electrolyte interphase (SEI) layer. Phosphite-based compounds tend to oxidize easily because the energy of their highest occupied molecular orbital (HOMO) is higher than that of the carbonate solvents in the electrolyte, such as ethylene carbonate (EC). Recently, substituted dioxaphosphinane was proposed as an oxidative additive to suppress the decomposition of the main electrolyte's components at the Li-rich cathode, $Li_{1.2}Ni_{0.18}Mn_{0.53}Co_{0.09}O_2$ ($0.5Li_2MnO_3 \cdot 0.5LiNi_{0.44}Co_{0.24}Mn_{0.32}O_2$).[41] Cells with substituted dioxaphosphinane-containing electrolyte could potentially have relatively low interfacial impedance, improved cycling stability, and thermally stable Li-rich cathodes. Lee reported that the additive triethyl phosphite (TEPi) improved the cycling performance of a $Li_{1.167}Ni_{0.233}Co_{0.1}Mn_{0.467}Mo_{0.033}O_2$ cathode and greatly reduced the internal cell pressure because TEPi may react with oxygen generated from the activation of Li_2MnO_3 in the $Li_{1.167}Ni_{0.233}Co_{0.1}Mn_{0.467}Mo_{0.033}O_2$ cathode.[42] Li's group investigated the effect of trimethyl phosphite (TMPi) on high-voltage Li-ion cells with a Li-rich layered oxide cathode, $Li_{1.2}Mn_{0.54}Ni_{0.13}Co_{0.13}O_2$. The cell with TMPi-added electrolyte exhibited good capacity retention, improved rate capability of Li-rich layered oxide/Li half cells at room temperature, and slightly enhanced thermal stability of the delithiated cathode in the presence of the electrolyte.[43] The nature of the SEI strongly affects not only the reversibility of electrochemical reactions of the cathode but also the kinetics of Li^+ transport through the cathode−electrolyte interface.[44] To the best of our knowledge, there are no systematic studies of the influence of the phosphite-based oxidative additive on the chemical and physical characteristics of the SEI formed on Li-rich cathodes, the dissolution of metal ions from the cathodes, and an irreversible phase transformation of the cathodes.

Herein, we demonstrate the beneficial impact of tris(trimethylsilyl) phosphite (TMSP) on the cycling performance and rate capability of a Li-rich cathode, $Li_{1.17}Ni_{0.17}Mn_{0.5}Co_{0.17}O_2$, in half cells and full cells coupled with a graphite anode. Moreover, the unique functions of TMSP with respect to the surface chemistry and phase transformation of Li-rich cathodes are precisely investigated by applying surface analyses based on *ex situ* X-ray photoelectron spectroscopy (XPS), high-resolution transmission electron microscopy (HR-TEM), and electron energy loss spectroscopy (EELS) measurements.

2. EXPERIMENTAL SECTION

2.1. Preparation of Electrolyte and Electrode. The electrolyte was prepared by dissolving 1.3 M lithium hexafluorophosphate ($LiPF_6$, Soulbrain Co. Ltd.) in a mixture of ethylene carbonate (EC), ethylmethyl carbonate (EMC), and dimethyl carbonate (DMC) in a 3:4:3 volume ratio. Another electrolyte was prepared by adding 0.5 wt % tris(trimethylsilyl) phosphite (TMSP, 95%, Aldrich) or 0.5 wt % trimethyl phosphite (TMPi, >99%, Aldrich) as an additive. The oxidation tendency of EC and TMSP was predicted by calculating the highest occupied molecular orbital (HOMO) with MOPAC, a semiempirical molecular orbital program (not shown here). For the electrochemical tests, the electrode was prepared by spreading a slurry mixture of 80 wt % $Li_{1.17}Ni_{0.17}Mn_{0.5}Co_{0.17}O_2$ ($0.5Li[Li_{1/3}Mn_{2/3}]O_2 \cdot 0.5LiNi_{1/3}Co_{1/3}Mn_{1/3}O_2$, Samsung Corning Precision Materials Co., Ltd.) as an active material, 10 wt % carbon black as a conducting material, and 10 wt % polyvinylidene fluoride (PVDF) binder dissolved in anhydrous *N*-methyl-2-pyrrolidineone (NMP, 99.5%, Aldrich). The slurry was cast on aluminum foil and dried in a convection oven at 80 °C for 30 min. After drying, the electrode was pressed and the thickness was around 45 μm. The specific capacity of the cathode and the active material loading were 0.99 mAh cm^{-2} and 4.97 mg cm^{-2}. The specific capacity of the cathode for a full cell coupled with the graphite anode was 2.24 mAh cm^{-2}. The anode was composed of 97.5 wt % natural graphite and 2.5 wt % binder (1.5 wt % styrene−butadiene rubber + 1 wt % sodium carboxymethyl cellulose). A microporous polyethylene film (PE, SK innovation Co. Ltd.) was used as a separator, and its thickness and porosity were 20 μm and 38%, respectively.

2.2. Electrochemical Measurements. Electrochemical tests were performed using 2032 coin-type half cells assembled in an argon-filled glovebox. Half cells with $Li_{1.17}Ni_{0.17}Mn_{0.5}Co_{0.17}O_2$ cathode and full cells with graphite anode and $Li_{1.17}Ni_{0.17}Mn_{0.5}Co_{0.17}O_2$ cathode were galvanostatically precycled at a rate of C/10 between 2.0 and 4.6 V using a computer-controlled battery measurement system (WonATech WBCS 3000). Thereafter, the cells were cycled at a current density of 100 mA g^{-1} (corresponding to C/2 rate) between 2.0 and 4.6 V for 100 cycles. To investigate the impact of TMSP on the rate capability of the $Li_{1.17}Ni_{0.17}Mn_{0.5}Co_{0.17}O_2$ cathodes, cathode half cells were cycled at various C rates: C/5, C/2, 1C, 2C, 3C, and 7C. dQ/dV graphs were obtained by computing the differential capacity versus the potential of the half cells during the precycle at 25 and 60 °C. To investigate the storage performance at high temperature, the graphite/$Li_{1.17}Ni_{0.17}Mn_{0.5}Co_{0.17}O_2$ full cells were galvanostatically precycled once between 2.0 and 4.6 V at a rate of C/10 at 25 °C. After the precycle, the cells were charged to 4.6 V with a constant current (CC) at a rate of C/10 followed by a constant voltage (CV) condition at 25 °C and then stored at 60 °C. The open-circuit voltage (OCV) variation of graphite/$Li_{1.17}Ni_{0.17}Mn_{0.5}Co_{0.17}O_2$ cells was monitored during storage, and the capacity retention was evaluated after 20 days.

2.3. Material Characterization. After precycling and 100 cycles, the cells were carefully disassembled in a glovebox to collect their electrodes and lithium metals. The electrodes and lithium metals were rinsed in dimethyl carbonate (DMC) to remove the residual $LiPF_6$-based electrolyte and dried at room temperature for *ex situ* analysis. The X-ray photoelectron spectroscopy (XPS, K-Alpha, Thermo Fisher) was performed with Al Kα ($h\nu$ = 1486.6 eV) radiation under ultrahigh vacuum, using a 0.10 eV step and 50 eV pass energy. All XPS spectra were calibrated by the hydrocarbon peak at the binding energy of 284.8 eV. All of the samples were prepared in a glovebox and sealed with an aluminum pouch film under vacuum before use. High-resolution transmission electron microscopy (TEM,

DOI: 10.1021/acsami.5b01770
ACS Appl. Mater. Interfaces 2015, 7, 8319−8329

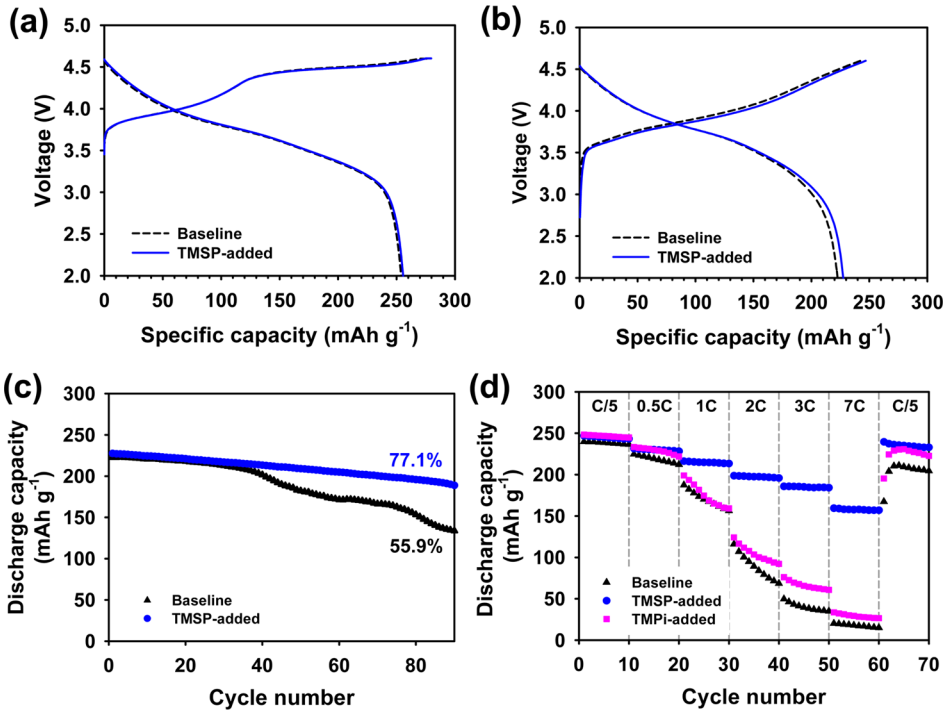

Figure 1. Voltage profiles of the Li/$Li_{1.17}Ni_{0.17}Mn_{0.5}Co_{0.17}O_2$ cells with and without TMSP additive at 25 °C in the (a) precycle and (b) first cycle after the precycle. (c) Cycling stability of Li/$Li_{1.17}Ni_{0.17}Mn_{0.5}Co_{0.17}O_2$ cells with and without TMSP additive at 25 °C. (d) Rate capability of $Li_{1.17}Ni_{0.17}Mn_{0.5}Co_{0.17}O_2$ in baseline electrolyte and the electrolyte with TMSP or TMPi additive at various C rates.

JEM-2100F, JEOL) was used to study the morphology of the SEI layer and $Li_{1.17}Ni_{0.17}Mn_{0.5}Co_{0.17}O_2$ particles. Using focused ion beam (FIB, Helios 450 HP, FEI) with both ion and electron beam, the TEM samples were prepared. Electron energy loss spectroscopy (EELS) was used to evaluate the valence state change of Mn ions, which is related to the capacity decay of the Li-rich cathode. TEM image and EELS spectra were acquired at 200 kV and the resolution of EELS was 0.8 eV. To clarify the role of TMSP and TMPi on HF removal from the electrolyte adding 5 vol % water, ^{19}F NMR spectra of the EC/EMC/DMC (3/4/3, v/v/v)/1 M $LiPF_6$ electrolytes with and without TMSP or TMPi were recorded on an Agilent VNMRS-600 spectrometer with THF-d8 as a solvent. ^{19}F NMR resonance was referenced to $LiPF_6$ at −72.4 ppm. To understand the dissolution behavior of transition metal ions such as manganese, nickel, and cobalt from $Li_{1.17}Ni_{0.17}Mn_{0.5}Co_{0.17}O_2$ cathodes at 60 °C, a typical experiment was performed. Fully charged cathodes with and without a TMSP-derived SEI layer were soaked in EC/EMC/DMC (3/4/3) with 1.3 M $LiPF_6$ under argon in a polyethylene bottle. After sealing with an aluminum pouch film, the polyethylene vial was stored in a convection oven at 60 °C for 24 h. The amount of manganese (Mn), nickel (Ni), and cobalt (Co) ions in the electrolyte that had come into contact with the fully charged cathode at 60 °C was measured by means of inductively coupled plasma-mass spectrometry (ICP/MS, ELAN DRC-II).

3. RESULTS AND DISCUSSION

Conventional carbonate-solvent-based electrolytes display inferior oxidation stability of lower than 4.3 V vs Li/Li^+, which makes them highly unstable against high-voltage cathodes. Therefore, understanding the interfacial characteristics between the high-voltage cathode and the electrolyte is critically important for developing suitable electrolytes. To examine the surface chemistry of Li-rich cathodes ($Li_{1.17}Ni_{0.17}Mn_{0.5}Co_{0.17}O_2$ activating Li_2MnO_3 at high voltages), *ex situ* XPS measurements of the cathodes were performed at various charged and discharged states, as shown in Figure S1 in the Supporting Information. At point i, the Ni^{2+} peak intensity at 855 eV was slightly reduced and the peak corresponding to Ni^{3+} appeared at 856 eV, as shown in Figure S1b in the Supporting Information.[45] Unfortunately, the peak attributed to Ni^{4+}, which is generated by delithiation of Li-rich cathodes, did not clearly appear at 860.9 eV (Figure S1b in the Supporting Information). At point ii, the Ni^{4+} peak intensity was apparently reduced (Figure S1c in the Supporting Information).[46] In the highly oxidized state, Ni^{4+} produced by the electrochemical oxidation of Ni^{2+} ions tends to take the electrons from the solvents and the electrons from the oxidative decomposition of solvents are probably consumed in the conversion of Ni^{4+} ions to Ni^{2+} on the cathode surface in contact with the electrolyte. The resulting Ni^{2+} ions are thought to form NiF_2 by the reaction with HF on the cathode surface. The intensity of the peak assigned to Ni^{2+} ions in the Li-rich cathode at a fully charged state (point ii) was lower, possibly because divalent Ni ions (Ni^{2+}) electrochemically oxidize to the tetravalent state (Ni^{4+}) through an intermediate stage of Ni^{3+} during charging (Figure S1c in the Supporting Information). During the subsequent discharge process, the resulting Ni^{4+} ions reduce to Ni^{2+} ions. Interestingly, the peak corresponding to NiF_2, located at 858 eV on the Li-rich cathode, fully discharged to 2.0 V vs Li/Li^+ (Figure S1e in the Supporting Information).[47] Metal fluorides such as NiF_2 can be generated by the reaction between Ni^{2+} and HF in the electrolyte. It should be noted that labile P−F bonds are highly susceptible to hydrolysis and generate HF even if trace amounts of moisture are present in the electrolyte solution ($LiPF_6$ (sol.) + H_2O → POF_3 (sol.) + LiF (s) + 2HF (sol.) and PF_5 (sol.) + H_2O → POF_3 (sol.) + 2HF (sol.)). The NiF_2 compound on the cathode may act as an electrical insulating material that inhibits electron transport and causes the cell resistance to increase.[48] Additionally, since NiF_2 formation means the loss of active materials, the reversible capacity of the cathode may decrease. Further evidence is given

DOI: 10.1021/acsami.5b01770
ACS Appl. Mater. Interfaces 2015, 7, 8319−8329

in the F 1s XPS spectra of Figure S1f in the Supporting Information. A pronounced peak attributed to NiF_2 at 685.1 eV[49] was observed for the cathode fully discharged to 2.0 V, whereas in the charged (points i and ii) and partially discharged (point iii) states, the LiF peak appeared at 684.3 eV on the cathode surface. From the XPS result, we could confirm that the NiF_2 insulating material is produced via the reaction of Ni^{2+} with HF in a fully discharge state (point iv). Since the characteristics of the surface layer formed on the cathode are key factors that affect the lithiation−delithiation kinetics and the interfacial stability during long-term cycling, we attempted to modify the surface chemistry of the Li-rich cathode using an electrolyte additive to form a desirable artificial SEI layer on the cathode surface. To stabilize the Li-rich cathode−electrolyte interface at high voltages, tris(trimethylsilyl) phosphite (TMSP) was selected as the functional oxidative additive. It should be noted that TMSP is prone to lose electrons in electrochemically oxidative environments because its HOMO energy (−8.097 eV) is higher than that of carbonate solvents (HOMO energy: EC = −11.905 eV, DMC = −11.821 eV, EMC = −11.541 eV), thus readily reacting with the HF in the electrolyte owing to its nonmaximal oxidation degree.[44]

Figure 1a shows the voltage profiles of Li/$Li_{1.17}Ni_{0.17}Mn_{0.5}Co_{0.17}O_2$ half cells with and without the TMSP additive at 25 °C. $Li_{1.17}Ni_{0.17}Mn_{0.5}Co_{0.17}O_2$ cathodes composed of Li_2MnO_3 and $Li(Ni_{1/3}Mn_{1/3}Co_{1/3})O_2$ showed two voltage plateaus (~4.0 and 4.5 V) during the precycle charge process and delivered a large reversible capacity of approximately 250 mAh g^{-1}. The discharge capacities of cathodes with and without TMSP were nearly identical at the precycle. It is known that the first voltage plateau at around 4.0 V indicates the delithiation of $Li(Ni_{1/3}Mn_{1/3}Co_{1/3})O_2$, and the second plateau at around 4.5 V represents the Li_2MnO_3 activation, which adds to the reversible capacity of the cathode.[15,16] The $Li_{1.17}Ni_{0.17}Mn_{0.5}Co_{0.17}O_2$ cathode with TMSP-added electrolyte had a similar initial Coulombic efficiency of 91.5% as the baseline electrolyte (91.8%). A comparison of the reversible capacity of the cathodes revealed that the discharge capacity of the baseline electrolyte is similar to that of TMSP-containing electrolyte in the first cycle after the precycle (Figure 1b).

These results suggest that the use of TMSP preserves the reversibility of electrochemical reactions of the $Li_{1.17}Ni_{0.17}Mn_{0.5}Co_{0.17}O_2$ cathode without significant capacity loss. More persuasive evidence for the positive impact of TMSP on the cycling stability of the cathode is given in Figure 1c. The discharge capacity retention of Li/$Li_{1.17}Ni_{0.17}Mn_{0.5}Co_{0.17}O_2$ half cells at a rate of C/2 was drastically improved from 55.9% to 77.1% by using the TMSP additive. It is thought that TMSP builds up a protective surface film that effectively inhibits transition metal dissoultion and continuous electrolyte decomposition at high voltages during cycling. Moreover, the TMSP-derived SEI layer on the cathode offers highly improved conduction pathways for Li ions and electrons to ensure superior cycling stability (Figure 1d). A comparison of the interfacial resistance of the cathodes cycled in the baseline and TMSP-added electrolytes is shown in Figure S2 in the Supporting Information. The interfacial resistance (67 Ω), including the SEI resistance and charge transfer resistance of cathodes with TMSP-containing electrolyte, is much lower than that of the baseline electrolyte (130 Ω) after the precycle (Figure S2a in the Supporting Information). This implies that the TMSP-derived SEI allows facile charge transfer through it. Furthermore, the AC impedance spectra in Figure S2b, Supporting Information, clearly show that the TMSP-added electrolyte forms a very low resistance SEI compared to the baseline electrolyte even after 100 cycles. More clear evidence for the role of the TMSP additive in forming low resistance SEI layers on the cathode is presented in Figure 1d. Since the voltage of the Li/$Li_{1.17}Ni_{0.17}Mn_{0.5}Co_{0.17}O_2$ half cells rapidly reaches the cutoff voltage (due to polarization at high C rates during the discharge process), the reversible capacity of the cathode may be reduced under a given voltage range. At high discharge rates, the $Li_{1.17}Ni_{0.17}Mn_{0.5}Co_{0.17}O_2$ cathode with TMSP-added electrolyte has a superior rate compared to the baseline electrolyte. The discharge capacity of the cathode with the baseline electrolyte started to decrease drastically at a rate of 1 C (corresponding to 200 mA g^{-1}) and was 156 mAh g^{-1} at the end of cycling at the 1 C rate. Unlike the baseline electrolyte, the $Li_{1.17}Ni_{0.17}Mn_{0.5}Co_{0.17}O_2$ cathode with TMSP-added electrolyte maintained a high discharge capacity of 195 mAh g^{-1} at a rate of 2 C. Surprisingly, the cathode with the TMSP-containing electrolyte delivered an excellent discharge capacity of over 150 mAh g^{-1} even at a high rate of 7 C. This stands in striking contrast to the trimethyl phosphite (TMPi)-added electrolyte exhibiting a very low discharge capacity of 34 mAh g^{-1} even at a high rate of 7 C (Figure 1d). To understand the different role of phosphite-based additives, TMSP and TMPi, on the Li^+ and electron transport through the cathode−electrolyte interface, their action for eliminating HF, which results in the NiF_2 formation acting as an electrical insulating material, was investigated, as shown in Figure 2.

The characteristic resonance of HF at −154.5 ppm was clearly observed in the electrolyte with TMPi, while the resonance of HF apparently disappeared in the TMSP-added

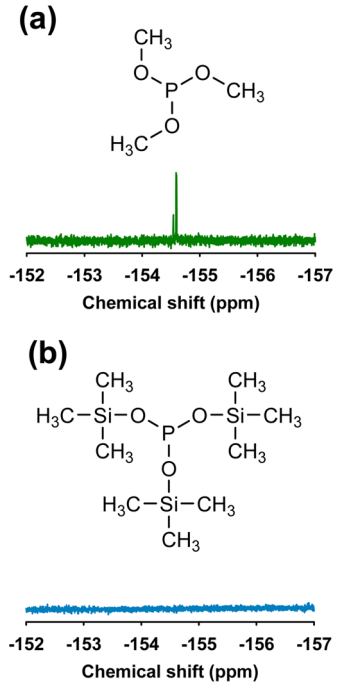

Figure 2. ^{19}F NMR spectra of the electrolytes with (a) 0.5% TMPi and (b) 0.5% TMSP. Five vol % water was added to the TMPi- and TMSP-added electrolyte solutions, and the ^{19}F NMR measurement of the resulting solutions stored for 22 h at room temperature was performed.

DOI: 10.1021/acsami.5b01770
ACS Appl. Mater. Interfaces 2015, 7, 8319−8329

electrolyte, as shown in the ^{19}F NMR spectra of Figure 2. This result implies that the ability of TMPi for the HF removal is relatively low compared to TMSP. Residual HF, which was not entirely eliminated by TMPi, may cause the NiF_2 formation by the reaction with Ni^{2+}. The cycling performance of full cells coupled with a graphite anode were examined over 100 cycles at 25 °C. Figure 3a clearly shows that the voltage profiles of

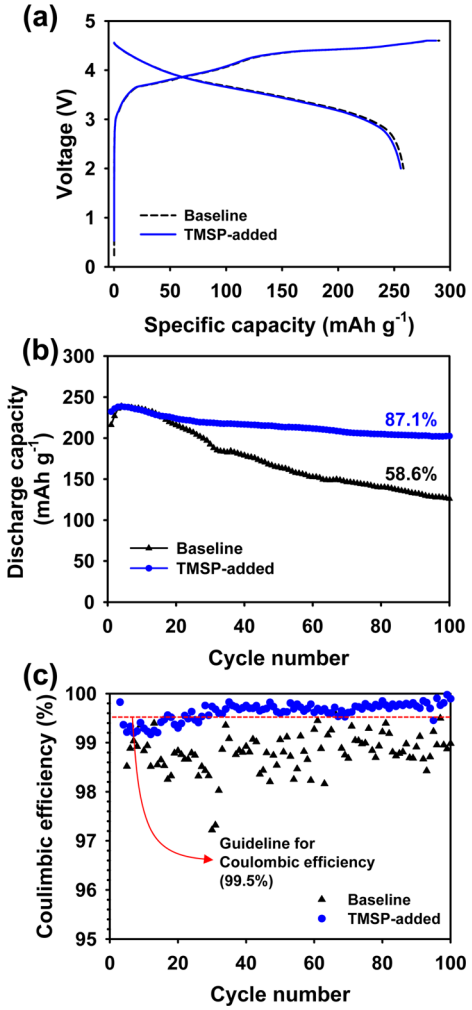

Figure 3. (a) Voltage profiles of graphite/$Li_{1.17}Ni_{0.17}Mn_{0.5}Co_{0.17}O_2$ full cells with and without 0.5% TMSP additive during the precycle. (b) Discharge capacity retention and (c) Coulombic efficiency of graphite/$Li_{1.17}Ni_{0.17}Mn_{0.5}Co_{0.17}O_2$ full cells with and without 0.5% TMSP additive at 25 °C.

graphite/$Li_{1.17}Ni_{0.17}Mn_{0.5}Co_{0.17}O_2$ full cells for both baseline and TMSP-added electrolytes are similar. Figure 3b,c shows a substantial improvement in the cycling stability and Coulombic efficiency of full cells with TMSP additive. The discharge capacity retention of full cells with the TMSP-containing electrolyte was drastically improved compared with the baseline electrolyte from 58.6% to 87.1% after 100 cycles at 25 °C. Moreover, a very high Coulombic efficiency of over 99.5%, which is vital for practical applications, was obtained for the full cell with TMSP, shown in Figure 3c. However, the capacity of the full cell with the baseline electrolyte faded rapidly during cycling and had a very unstable, low Coulombic efficiency below 99%. This low Coulombic efficiency may have originated from two side reactions: First, the cracked SEI layer on the anode can be repaired, resulting in a net consumption of Li from cathode. Second, the reformation of SEI, which is dissolved from the anode and is oxidized at the cathode, takes place.[50] This may be because of unwanted electrolyte decomposition at the cathode cycled with a high voltage of 4.6 V in a full cell and the loss of reversible capacity by metal (Ni, Mn, Co) deposition on the graphite. We speculate that the metal ions dissolved out of the cathode may cause the capacity of a full cell to fade considerably because the dissolved metal ions migrate toward the graphite anode under an electric field and the deposition of metal ions leading to the extraction of Li^+ ions from the lithiated graphite anode occurs.[51] This finding suggests that severe oxidative decomposition of the electrolyte caused by the high charge cutoff voltage (4.6 V) and the dissolution of metal ions by HF attack are effectively reduced by using the TMSP additive. Potential surface chemistry mechanisms of the TMSP additive are proposed in Figure 4.

To investigate the surface chemistry mechanisms of the cathode with and without the TMSP additive, *ex situ* X-ray photoelectron spectroscopy (XPS) was performed after the precycle at 25 °C. Figure 5 shows the P 2p, F 1s, and O 1s XPS spectra for the cathodes with and without the TMSP additive. A pronounced peak corresponding to P−O containing compounds appeared at 134.2 eV, slightly higher than the binding energy of $Li_xPO_yF_z$ (~134 eV), as shown in Figure 5b. This P−O group may be produced by decomposition of TMSP at the cathode (see schematic of Figure 4); therefore, TMSP may contribute to the formation of the SEI on the cathode. Our previous investigation of 5 V class high voltage LNMO cathodes with and without TMSP clearly showed that TMSP eliminates HF from the electrolyte and forms a stable and robust SEI on the cathode.[44]

The F 1s XPS spectra of Figure 5 show two major peaks; one corresponds to the P−F bond formed by $LiPF_6$ decomposition and the other is attributed to LiF created by the reaction of HF with Li ions and the SEI component, such as Li_2CO_3 ($2HF + Li_2CO_3 \rightarrow 2LiF + H_2O + CO_2\uparrow$). In the case of the cathode precycled in the TMSP-added electrolyte, the LiF peak was discernibly lower. This means that TMSP effectively mitigates LiF formation by eliminating HF from the electrolyte, as depicted in Figure 4. In addition, the cathode with TMSP additive exhibits a more intense peak at 530 eV, compared to the baseline electrolyte (O 1s spectra of Figure 5), which is assigned to metal oxide (M-O) of the cathode. This is probably because the TMSP-derived SEI is thinner than the SEI formed by the baseline electrolyte and therefore does not block the cathode surface as much.

As previously mentioned in Figure S1e,f, Supporting Information, the NiF_2 peak was observed on the cathode with the baseline electrolyte in the fully discharged state during the precycle. Interestingly, the NiF_2 peak mostly disappeared for the cathode precycled in the TMSP-added electrolyte, as clearly shown in the Ni 2p XPS spectra of Figure 6. The HF can react with Ni^{2+} ions produced during the discharge process which results in the formation of NiF_2 on the cathode ($Ni^{2+} + 2HF \rightarrow NiF_2 + H_2\uparrow$). Since the TMSP additive can act as a scavenger for HF in the electrolyte (see the schematic of Figure 4 and ^{19}F NMR of Figure 2b), the formation of NiF_2 on the cathode with TMSP could be suppressed and thus the capacity loss via the NiF_2 formation could be minimized. Although HF is not entirely removed from the electrolyte, the TMSP-derived SEI layer is expected to block the HF attack toward the cathode, as seen in the schematic representation of Figure 4.

DOI: 10.1021/acsami.5b01770
ACS Appl. Mater. Interfaces 2015, 7, 8319−8329

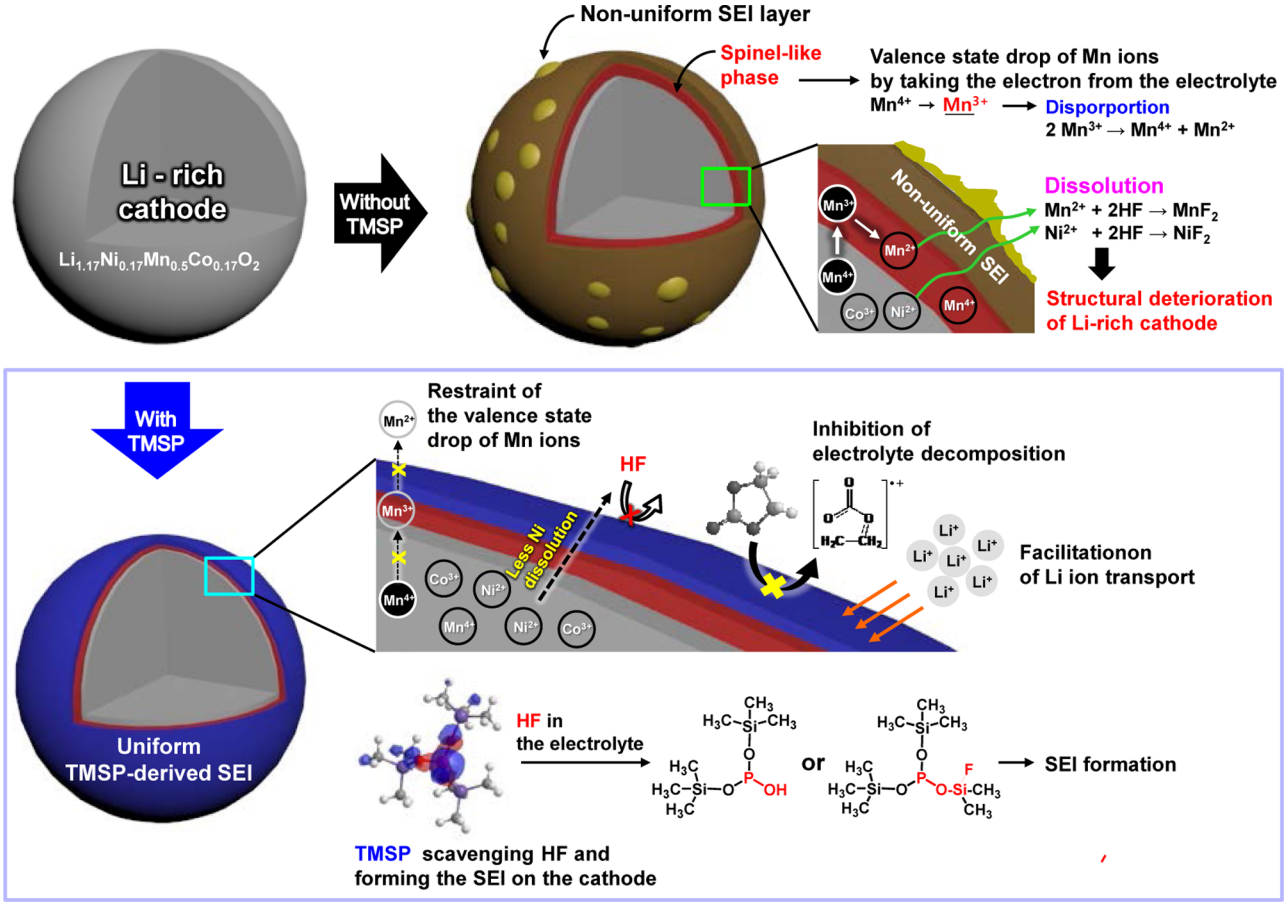

Figure 4. A schematic representation showing the problems induced by the baseline electrolyte and the unique functions of the TMSP additive for high-performance Li-rich cathodes.

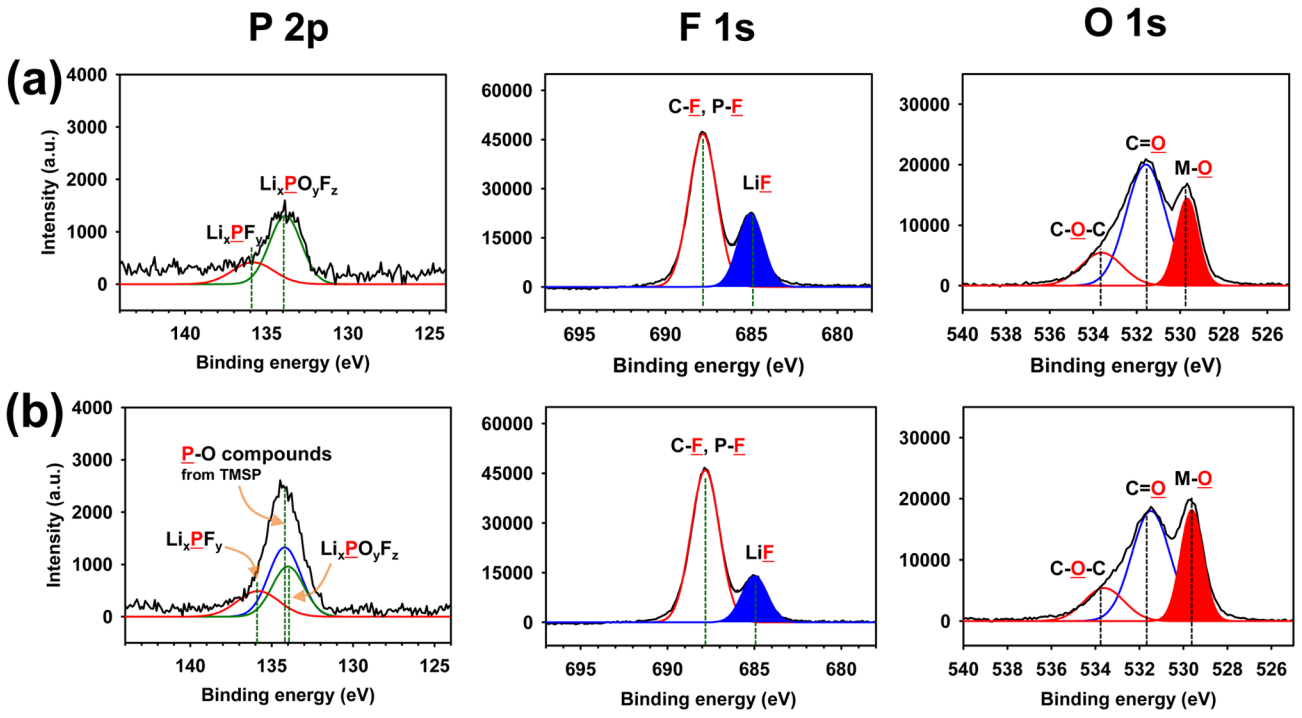

Figure 5. P 2p, F 1s, and O 1s XPS spectra for the $Li_{1.17}Ni_{0.17}Mn_{0.5}Co_{0.17}O_2$ cathodes precycled in (a) baseline electrolyte and (b) TMSP-added electrolyte.

DOI: 10.1021/acsami.5b01770
ACS Appl. Mater. Interfaces 2015, 7, 8319−8329

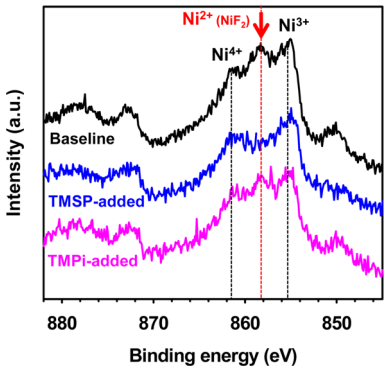

Figure 6. Ni 2p XPS spectra for the $Li_{1.17}Ni_{0.17}Mn_{0.5}Co_{0.17}O_2$ cathodes precycled in baseline electrolyte and the electrolyte with TMSP or TMPi additive.

On the other hand, a peak corresponding to NiF_2 at 685.1 eV appeared for the $Li_{1.17}Ni_{0.17}Mn_{0.5}Co_{0.17}O_2$ cathode precycled in the electrolyte with TMPi additive, as displayed in Figure 6. This is because the TMPi additive did not effectively eliminate HF compared to TMSP, as presented in Figure 2a,b.

High-resolution transmission electron microscopy (HR-TEM) was used to investigate the physical structure of the SEI layer on the cathode. Figure 7 shows the representative morphology of the SEI layer on the cathode with and without TMSP additive after 50 cycles. We found that the baseline electrolyte forms a thick, nonuniform, and bumpy SEI layer that covers the cathode particles. A thick SEI layer may hamper the transport of lithium ions and electrons inside the cathode and thereby impede the kinetics of delithiation and lithiation of the cathode upon prolonged cycling. However, the cathode cycled in the TMSP-added electrolyte was evenly covered with a thin SEI layer (<6 nm). This is persuasive evidence that the TMSP additive forms a uniform SEI layer on the cathode surface, which allows facile charge transport and prevents severe electrolyte decomposition in highly oxidative conditions induced by the high charge voltage of 4.6 V. Another critical issue for the failure mechanism of Li-rich cathodes during cycling is phase transformation from a layered to spinel-like phase.[23−28] The main cause of phase transformation is cation disorder through the migration of transition metal ions in the transition metal layer to Li vacancies in the Li layer.[28] Phase transformation causes capacity fading because transition metal ions in the Li layer disturb the lithiation or delithiation process. Therefore, suppression of the phase transformation from layered to spinel could be a highly effective strategy to improve the cycling performance of Li-rich cathodes.

To elucidate the positive effect that the TMSP-added electrolyte has on the surface chemistry and phase transformation of the $Li_{1.17}Ni_{0.17}Mn_{0.5}Co_{0.17}O_2$ cathode during cycling, electron energy loss spectroscopy (EELS) was performed, as shown in Figure 8. The change of Mn ion valence states can be explained on the basis of the peak shift in the EELS result. Compared with the cathode bulk, the Mn L edge clearly shows a chemical shift of 2.8 eV toward lower energy for the cathode surface cycled in baseline electrolyte (Figure 8c). This indicates that the valence state of Mn ions is 2+ for the cycled cathode surface, whereas after 50 cycles, the valence state of Mn ions is 4+ in the cathode bulk. This result is in good agreement with previous results, where the inhomogeneous valence state of Mn ions was observed with its lower oxidation state near surface than in the bulk, causing a severe capacity decay of the Li-rich cathode.[23,27] The lower Mn ion valence is possibly because the disproportion reaction of Mn^{3+} ions takes place because of structural instabilities in the spinel-like phase. The disproportion reaction of Mn^{3+} ions ($2Mn^{3+}$ (spinel-like phase) → Mn^{4+} ($Li_2Mn_3O_7$) + Mn^{2+} (MnO or MnF_2)) in the spinel-like phase can produce a low Mn ion valence state, Mn^{2+}.[27,52] This process may propagate gradually from the surface to the bulk of the cathode as cycling progresses.[23,27] Thus, the inhomogeneous valence state of Mn ions could be one of the governing factors, which affect the degradation of the reversible capacity of Li-rich cathodes. Importantly, the chemical shift of the cathode surface cycled in the TMSP added electrolyte was reduced by 1.9 eV compared with the cathode bulk (Figure 8d). The Mn-L_3/L_2 ratio could be one of the indexes that represent the valence state change of Mn ions. For comparison between the bulk and the surface of the cycled cathode with the baseline electrolyte, the Mn L edges were normalized to the L_3 peak. The Mn-L_3/L_2 ratio of the cycled cathode surface decreased from 3.43 to 2.47 by using the TMSP additive (Figure 8c,d). The increment in the Mn-L_3/L_2 ratio with the addition of TMSP suggests that the TMSP-derived SEI effectively suppressed the valence state drop of Mn ions (for instance, the reduction of Mn^{4+} to Mn^{3+} by taking the electrons from the oxidative decomposition of the electrolyte)[53] as depicted in Figure 4. Mn^{3+} undergoes a disproportion reaction releasing Mn^{2+} of low Mn ion valence state and yielding Mn^{4+} ions. The released Mn^{2+} ions may migrate toward the counter electrode (the graphite anode in a full cell) and precipitate on the cathode surface via the reaction with F^- and O_2^- ions. These behaviors were suppressed by the TMSP-

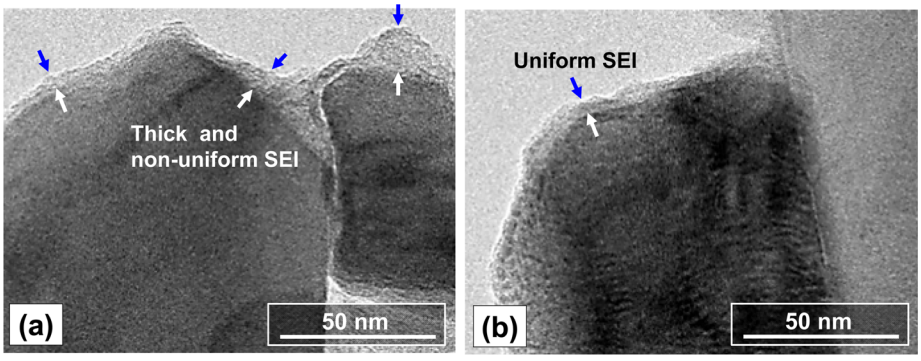

Figure 7. HR-TEM images of $Li_{1.17}Ni_{0.17}Mn_{0.5}Co_{0.17}O_2$ particle after 50 cycles in (a) baseline electrolyte and (b) TMSP-added electrolyte.

DOI: 10.1021/acsami.5b01770
ACS Appl. Mater. Interfaces 2015, 7, 8319−8329

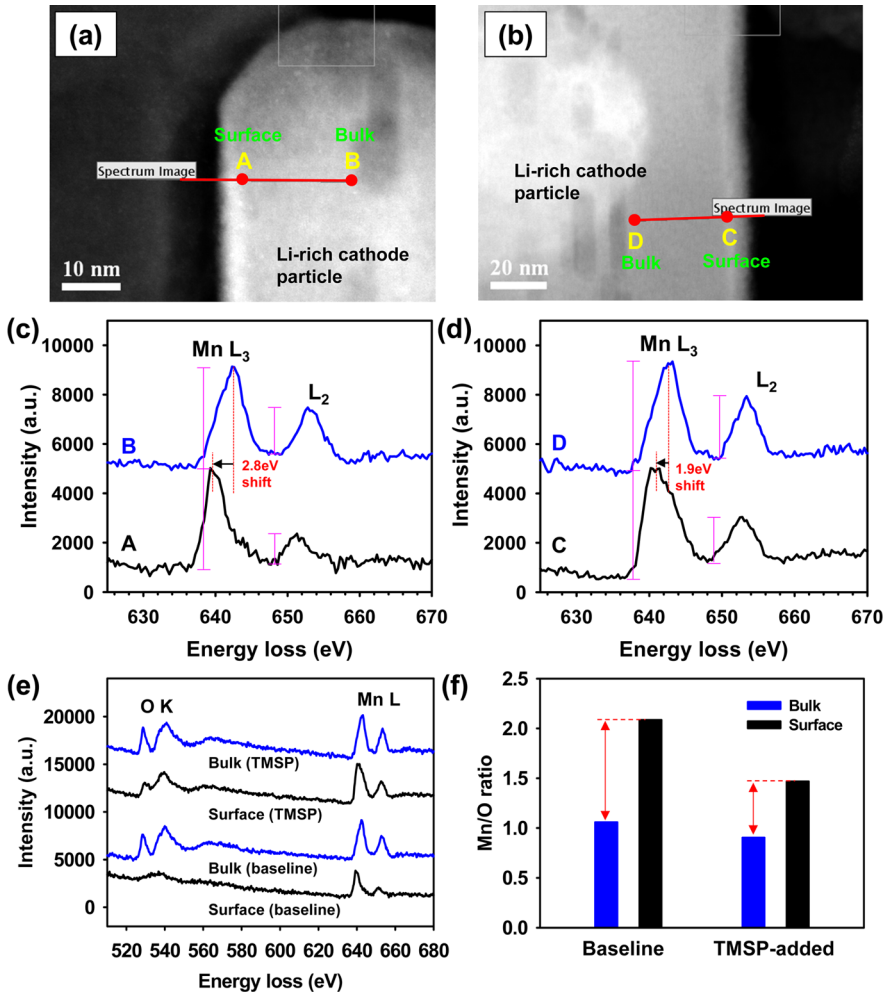

Figure 8. Scanning transmission electron microscopy (STEM) images of the $Li_{1.17}Ni_{0.17}Mn_{0.5}Co_{0.17}O_2$ cathode with (a) baseline and (b) TMSP-added electrolytes after 50 cycles. A and C represent the region underneath the SEI layer on the cathode surface. EELS spectra of the Mn L edge from the surface (black line) and bulk (blue line) of the $Li_{1.17}Ni_{0.17}Mn_{0.5}Co_{0.17}O_2$ cathodes with (c) baseline and (d) TMSP-added electrolytes after 50 cycles. For comparison, the Mn L edge was normalized to the Mn L3 peak. (e) O K and Mn L EELS spectra of the cycled cathode bulk and surface with and without TMSP additive. (f) Mn/O ratio of the cycled cathode bulk and surface with and without TMSP additive was calculated by integration of the O K and Mn L edge.

derived SEI on the Li-rich cathode (Figure 4), since the Mn-L_3/L_2 ratio was reduced compared to the baseline electrolyte. This behavior was further supported by the O K edge at ~527 eV that is closely linked to valence states of transition metal ions because the peak intensity of the O K edge reflects the local vacant 3d transition metal states.[23,27] The O K peaks for the cathode particles cycled in the baseline electrolyte almost disappeared, whereas the O K peaks for the cathode with TMSP-added electrolyte were clearly observed (Figure 8e). Our finding indicates that the valence states of the cycled particle surface transition metal (Mn) ions are significantly reduced in the baseline electrolyte, compared to the TMSP-added electrolyte. In other words, the TMSP-derived SEI effectively mitigates the Mn valence state drop ($Mn^{4+} \rightarrow Mn^{3+}$, Mn^{2+}), retards irreversible phase transformation from the layered to spinel-like phase, and improves the cycling stability of the Li-rich cathode. Although the phase transformation from layered to spinel-like was not completely avoided by using the TMSP additive, the dissolution of Mn^{2+} ions from the spinel-like phase of the cathode into the electrolyte is expected to be restrained by the TMSP-derived SEI layer on the cathode, as depicted in Figure 4. Since soluble Mn^{2+} ions readily react with HF to form MnF_2 on the cathode and cause significant capacity fading of the spinel-like phase in the cathode materials, practical methods, which suppress the dissolution of Mn^{2+} ions from the cathode, should be proposed to ensure the cycling performance of the Li-rich cathode. In this regard, the formation of a protective film on the cathode by using the TMSP additive is expected to be a very promising approach for high-performance Li-rich cathodes. Furthermore, the oxygen loss from the cathode surface is known to be a critical problem causing the capacity fading of Li-rich cathodes.[25,54,55] Therefore, it is important to minimize the oxygen loss of the Li-rich cathode caused by the valence state reduction of Mn ions ($Mn^{4+} + e^- \rightarrow Mn^{3+}$, $2Mn^{3+} \rightarrow Mn^{4+} + Mn^{2+}$, $Mn^{2+} + O^{2-}$ (from the cathode) $\rightarrow$ MnO↓ or $Ni^{2+} + O^{2-}$ (from the cathode) $\rightarrow$ NiO[28]). By integrating the area of Mn L and O K edge peaks and calculating the Mn/O ratio, we could quantitatively compare the oxygen loss for both cycled cathodes. As shown in Figure 8f, the Mn/O ratio for the surface of cathodes cycled in the baseline electrolyte is almost twice that of TMSP-added electrolyte. This indicates that the oxygen loss from the cathode can be suppressed by forming the protective layer on the cathode.

DOI: 10.1021/acsami.5b01770
ACS Appl. Mater. Interfaces 2015, 7, 8319−8329

To further understand the transition metal (Mn, Ni, Co) dissolution behavior of cycled Li-rich cathodes with and without TMSP-derived SEI, fully delithiated cathodes after the precycle were soaked in the electrolyte and stored at 60 °C for 24 h. The amount of transition metal ions in the baseline electrolyte was measured using inductively coupled plasma (ICP)-mass spectrometry (Figure 9). The electrolyte in contact

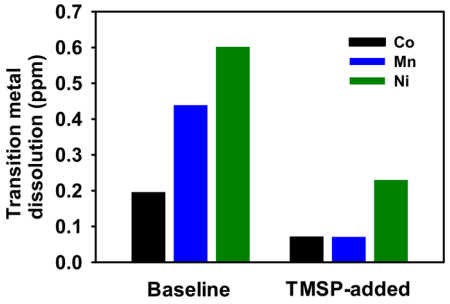

Figure 9. A comparison of transition metal dissolution behavior from the cycled Li-rich cathode with and without a TMSP-derived SEI. Fully delithiated cathodes with and without the TMSP-derived SEI were stored in the baseline electrolyte at 60 °C for 24 h.

with the cathode covered by the TMSP-derived SEI layer had a relatively low transition metal ion content compared to the cathode with the SEI formed by the baseline electrolyte. This is because the TMSP-derived SEI layer is robust enough to suppress the Ni/Mn/Co dissolution from the Li-rich cathode at 60 °C. On a basis of the HR-TEM and EELS studies, we believe that our proposed cathode surface chemistry mechanisms, with and without the TMSP additive, are reasonable, as previously displayed in Figure 4. The cathode with the baseline electrolyte suffers from considerable electrolyte decomposition at high voltages while HF attack promotes the dissolution of metal ions from the cathode (Figures 7 and 9). In addition, a nonuniform and thick SEI layer generated by the baseline electrolyte covers the cathode particles, whereas the TMSP-added electrolyte forms a highly uniform and thin SEI layer on the cathode surface. The resulting TMSP-originated SEI layer could reduce unwanted electrolyte decomposition in the highly oxidative environment and inhibit the formation of metal fluorides such as NiF_2 and MnF_2 that may be produced from the reaction between metal ions and HF (Figures 4 and 6). The dQ/dV measurement during the precycle at 25 and 60 °C shows that TMSP hinders electrolyte decomposition at high voltages. As shown in Figure S3 in the Supporting Information, the anodic peak caused by severe electrolyte oxidative decomposition appeared at around 4.6 V for the cathode precycled in the baseline electrolyte, while there was no appreciable anodic peak above 4.5 V for the cathode with the TMSP-added electrolyte (Figure S3 in the Supporting Information). It is clear that the baseline electrolyte undergoes significant oxidative decomposition, which resulted in a pronounced anodic peak at around 4.6 V during the precycle at 60 °C. This is because the baseline electrolyte is prone to electrochemical oxidation at high voltages and therefore severe oxidative decomposition is unavoidable.

The high temperature storage performance of graphite/$Li_{1.17}Ni_{0.17}Mn_{0.5}Co_{0.17}O_2$ full cells with and without TMSP was investigated at 60 °C for 20 days, as displayed in Figure 10. There was a significant open-circuit voltage (OCV) drop from 4.18 to 3.74 V in the full cell with the baseline electrolyte. However, unlike the baseline electrolyte, the TMSP-added electrolyte led to a slight OCV drop from 4.19 to 4.01 V in the full cell (Figure 10a). The full cell with TMSP had superior capacity retention (74.6%) after being stored at 60 °C for 20 days, compared to cells with the baseline electrolyte (53.8%) (Figure 10b). This indicates that TMSP-derived SEI on the cathode is thermally stable and robust enough to prevent continuous electrolyte decomposition and relithiation of the cathode induced by the breakdown of the SEI on the cathode. In addition, it is thought that the TMSP-originated SEI restrains the dissolution of transition metal ions from the cathode and thereby avoids the detrimental effects of the dissolved transition metal ions in a cell.

4. CONCLUSIONS

We demonstrated that the TMSP-derived SEI layer is a highly promising means to inhibit severe electrolyte decomposition at high voltages and leads to the substantially enhanced electrochemical performance of Li-rich layered cathodes. *Ex situ* XPS and TEM analyses confirmed that the TMSP additive forms a thin protective film that evenly covers the cathode surface. The *ex situ* EELS study manifested that the resultant TMSP-derived SEI layer effectively minimized structural disintegration of the Li-rich cathode surface during cycling. Furthermore, high-temperature storage performance tests of graphite/$Li_{1.17}Ni_{0.17}Mn_{0.5}Co_{0.17}O_2$ full cells at 60 °C clearly showed that the TMSP-originated SEI layer is essential to suppress the dissolution of metal ions from the cathode and to protect the graphite anode from the detrimental effects of metal deposition. We believe that the results of this study and the associated analysis will contribute to the design of suitable

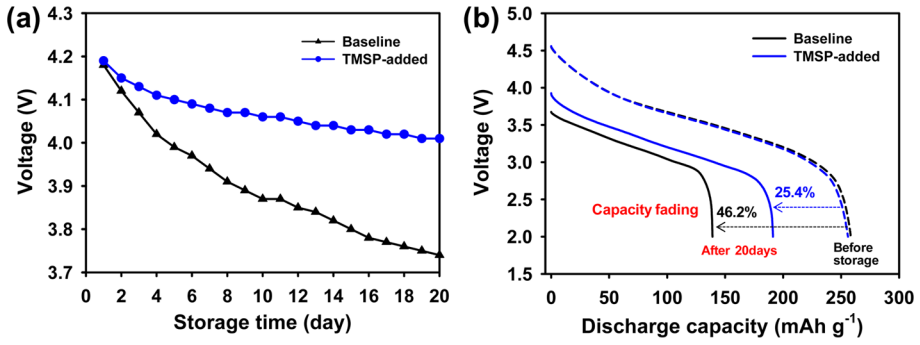

Figure 10. (a) OCV variation of graphite/$Li_{1.17}Ni_{0.17}Mn_{0.5}Co_{0.17}O_2$ full cells with and without TMSP additive at 60 °C with storage time. (b) Comparison of capacity retention of graphite/$Li_{1.17}Ni_{0.17}Mn_{0.5}Co_{0.17}O_2$ full cells with and without TMSP additive after storage at 60 °C for 20 days.

DOI: 10.1021/acsami.5b01770
ACS Appl. Mater. Interfaces 2015, 7, 8319−8329

additives with the promise of further improvements in electrochemical performance of Li-rich cathodes.

■ ASSOCIATED CONTENT

Supporting Information

AC impedance spectra of the Li/$Li_{1.17}Ni_{0.17}Mn_{0.5}Co_{0.17}O_2$ half cells with and without the TMSP additive, ^{19}F NMR spectra of the electrolytes with TMPi and TMSP, comparison of transition metal dissolution behavior from the cycled Li-rich cathode with and without a TMSP-derived SEI, dQ/dV graphs of $Li_{1.17}Ni_{0.17}Mn_{0.5}Co_{0.17}O_2$ cathodes with and without the TMSP additive. This material is available free of charge via the Internet at http://pubs.acs.org.

■ AUTHOR INFORMATION

Corresponding Authors

*E-mail: ktlee@unist.ac.kr

*E-mail: nschoi@unist.ac.kr.

Author Contributions

The manuscript was written through contributions of all authors. All authors have given approval to the final version of the manuscript.

Notes

The authors declare no competing financial interest.

■ ACKNOWLEDGMENTS

This research was supported by the IT R&D program of MOTIE/KEIT(KI001810046309) and by a grant from the Energy Efficiency & Resources of the Korea Institute of Energy Technology Evaluation and Planning (Project no. 20112010100140) funded by the Korean Ministry of Knowledge Economy. This study was partly supported by a National Research Foundation of Korea Grant funded by the Korean Government (MEST) (NRF-2013-C1AAA001-0030538) and by Industrial Strategic technology development program, (Project No. 10050477, Development of separator with low thermal shrinkage and electrolyte with high ionic conductivity for Na-ion batteries) funded by the Ministry of Trade, Industry & Energy (MI, Korea).

■ REFERENCES

(1) Tanaka, T.; Ohta, K.; Arai, N. Year 2000 R&D Status of Large-Scale Lithium Ion Secondary Batteries in the National Project of Japan. *J. Power Sources* **2001**, *97–8*, 2–6.

(2) Tarascon, J. M.; Armand, M. Issues and Challenges Facing Rechargeable Lithium Batteries. *Nature* **2001**, *414*, 359–367.

(3) Armand, M.; Tarascon, J. M. Building Better Batteries. *Nature* **2008**, *451*, 652–657.

(4) Scrosati, B.; Garche, J. Lithium Batteries: Status, Prospects and Future. *J. Power Sources* **2010**, *195*, 2419–2430.

(5) Yoo, H. D.; Markevich, E.; Salitra, G.; Sharon, D.; Aurbach, D. On the Challenge of Developing Advanced Technologies for Electrochemical Energy Storage and Conversion. *Mater. Today* **2014**, *17*, 110–121.

(6) Tollefson, J. Car Industry: Charging up the Future. *Nature* **2008**, *456*, 436–440.

(7) Goodenough, J. B.; Kim, Y. Challenges for Rechargeable Li Batteries. *Chem. Mater.* **2010**, *22*, 587–603.

(8) Su, L. W.; Jing, Y.; Zhou, Z. Li ion Battery Materials with Core-Shell Nanostructures. *Nanoscale* **2011**, *3*, 3967–3983.

(9) Hu, M.; Pang, X. L.; Zhou, Z. Recent Progress in High-Voltage Lithium Ion Batteries. *J. Power Sources* **2013**, *237*, 229–242.

(10) Julien, C. M.; Mauger, A. Review of 5-V Electrodes for Li-Ion Batteries: Status and Trends. *Ionics* **2013**, *19*, 951–988.

(11) Kim, J. H.; Pieczonka, N. P. W.; Yang, L. Challenges and Approaches for High-Voltage Spinel Lithium-Ion Batteries. *ChemPhysChem* **2014**, *15*, 1940–1954.

(12) Yabuuchi, N.; Yoshii, K.; Myung, S. T.; Nakai, I.; Komaba, S. Detailed Studies of a High-Capacity Electrode Material for Rechargeable Batteries, Li_2MnO_3-$LiCo_{1/3}Ni_{1/3}Mn_{1/3}O_2$. *J. Am. Chem. Soc.* **2011**, *133*, 4404–4419.

(13) Yu, H. J.; Zhou, H. S. High-Energy Cathode Materials (Li_2MnO_3-$LiMO_2$) for Lithium-Ion Batteries. *J. Phys. Chem. Lett.* **2013**, *4*, 1268–1280.

(14) Lu, Z. H.; MacNeil, D. D.; Dahn, J. R. Layered Cathode Materials $Li[Ni_xLi_{(1/3-2x/3)}Mn_{(2/3-x/3)}]O_2$ for Lithium-Ion Batteries. *Electrochem. Solid-State Lett.* **2001**, *4*, A191–A194.

(15) Lu, Z. H.; Dahn, J. R. Understanding the Anomalous Capacity of Li/$Li[Ni_xLi_{(1/3-2x/3)}Mn_{(2/3-x/3)}]O_2$ Cells Using in Situ X-ray Diffraction and Electrochemical Studies. *J. Electrochem. Soc.* **2002**, *149*, A815–A822.

(16) Kang, S. H.; Sun, Y. K.; Amine, K. Electrochemical and ex Situ X-ray Study of Li-$(Li_{0.2}Ni_{0.2}Mn_{0.6})O_2$ Cathode Material for Li Secondary Batteries. *Electrochem. Solid-State Lett.* **2003**, *6*, A183–A186.

(17) Robertson, A. D.; Bruce, P. G. Mechanism of Electrochemical Activity in Li_2MnO_3. *Chem. Mater.* **2003**, *15*, 1984–1992.

(18) Yu, D. Y. W.; Yanagida, K.; Kato, Y.; Nakamura, H. Electrochemical Activities in Li_2MnO_3. *J. Electrochem. Soc.* **2009**, *156*, A417–A424.

(19) Yu, S. H.; Yoon, T.; Mun, J.; Park, S.; Kang, Y. S.; Park, J. H.; Oh, S. M.; Sung, Y. E. Continuous Activation of Li_2MnO_3 Component upon Cycling in $Li_{1.167}Ni_{0.233}Co_{0.100}Mn_{0.467}Mo_{0.033}O_2$ Cathode Material for Lithium Ion Batteries. *J. Mater. Chem. A* **2013**, *1*, 2833–2839.

(20) Yu, C.; Li, G. S.; Guan, X. F.; Zheng, J.; Luo, D.; Li, L. P. The Impact of Upper Cut-Off Voltages on the Electrochemical Behaviors of Composite Electrode $0.3Li_2MnO_3$ Center Dot $0.7LiMn_{1/3}Ni_{1/3}Co_{1/3}O_2$. *Phys. Chem. Chem. Phys.* **2012**, *14*, 12368–12377.

(21) Ye, D. L.; Ozawa, K.; Wang, B.; Hulicova-Jurcakova, D.; Zou, J.; Sun, C. H.; Wang, L. Z. Capacity-Controllable Li-Rich Cathode Materials for Lithium-Ion Batteries. *Nano Energy* **2014**, *6*, 92–102.

(22) Thackeray, M. M.; Kang, S. H.; Johnson, C. S.; Vaughey, J. T.; Benedek, R.; Hackney, S. A. Li_2MnO_3-Stabilized $LiMO_2$ (M = Mn, Ni, Co) Electrodes for Lithium-Ion Batteries. *J. Mater. Chem.* **2007**, *17*, 3112–3125.

(23) Xu, B.; Fell, C. R.; Chi, M. F.; Meng, Y. S. Identifying Surface Structural Changes in Layered Li-Excess Nickel Manganese Oxides in High Voltage Lithium Ion Batteries: A Joint Experimental and Theoretical Study. *Energy Environ. Sci.* **2011**, *4*, 2223–2233.

(24) Yu, H. J.; Kim, H. J.; Wang, Y. R.; He, P.; Asakura, D.; Nakamura, Y.; Zhou, H. S. High-Energy 'Composite' Layered Manganese-Rich Cathode Materials via Controlling Li_2MnO_3 Phase Activation for Lithium-Ion Batteries. *Phys. Chem. Chem. Phys.* **2012**, *14*, 6584–6595.

(25) Boulineau, A.; Simonin, L.; Colin, J. F.; Bourbon, C.; Patoux, S. First Evidence of Manganese-Nickel Segregation and Densification upon Cycling in Li-Rich Layered Oxides for Lithium Batteries. *Nano Lett.* **2013**, *13*, 3857–3863.

(26) Gu, M.; Belharouak, I.; Zheng, J. M.; Wu, H. M.; Xiao, J.; Genc, A.; Amine, K.; Thevuthasan, S.; Baer, D. R.; Zhang, J. G.; Browning, N. D.; Liu, J.; Wang, C. M. Formation of the Spinel Phase in the Layered Composite Cathode Used in Li-Ion Batteries. *ACS Nano* **2013**, *7*, 760–767.

(27) Zheng, J. M.; Gu, M.; Xiao, J.; Zuo, P. J.; Wang, C. M.; Zhang, J. G. Corrosion/Fragmentation of Layered Composite Cathode and Related Capacity/Voltage Fading during Cycling Process. *Nano Lett.* **2013**, *13*, 3824–3830.

(28) Oh, P.; Ko, M.; Myeong, S.; Kim, Y.; Cho, J. A Novel Surface Treatment Method and New Insight into Discharge Voltage Deterioration for High-Performance $0.4Li_2MnO_3$–$0.6LiNi_{1/3}Co_{1/3}Mn_{1/3}O_2$ Cathode Materials. *Adv. Energy Mater.* **2014**, *4*, 1400631–1400639.

DOI: 10.1021/acsami.5b01770
ACS Appl. Mater. Interfaces 2015, 7, 8319–8329

(29) Xu, K. Nonaqueous Liquid Electrolytes for Lithium-Based Rechargeable Batteries. *Chem. Rev.* **2004**, *104*, 4303−4417.
(30) Yang, L.; Ravdel, B.; Lucht, B. L. Electrolyte Reactions with the Surface of High Voltage $LiNi_{0.5}Mn_{1.5}O_4$ Cathodes for Lithium-Ion Batteries. *Electrochem. Solid-State Lett.* **2010**, *13*, A95−A97.
(31) Chen, Z. H.; Sun, Y. K.; Amine, K. Electrochemical Properties of Lithium-Rich $Li_{1+x}(Mn_{1/3}Ni_{1/3}Co_{1/3})_{1-x}O_2$ at High Potential. *J. Electrochem. Soc.* **2006**, *153*, A1818−A1822.
(32) Li, Y.; Bettge, M.; Polzin, B.; Zhu, Y.; Balasubramanian, M.; Abraham, D. P. Understanding Long-Term Cycling Performance of $Li_{1.2}Ni_{0.15}Mn_{0.55}Co_{0.1}O_2$-Graphite Lithium-Ion Cells. *J. Electrochem. Soc.* **2013**, *160*, A3006−A3019.
(33) Zou, G. S.; Yang, X. K.; Wang, X. Y.; Ge, L.; Shu, H. B.; Bai, Y. S.; Wu, C.; Guo, H. P.; Hu, L.; Yi, X.; Ju, B. W.; Hu, H.; Wang, D.; Yu, R. Z. Improvement of Electrochemical Performance for Li-Rich Spherical $Li_{1.3}[Ni_{0.35}Mn_{0.65}]O_{2+x}$ Modified by Al_2O_3. *J. Solid State Electrochem.* **2014**, *18*, 1789−1797.
(34) Wang, Z. Y.; Liu, E. Z.; Guo, L. C.; Shi, C. S.; He, C. N.; Li, J. J.; Zhao, N. Q. Cycle Performance Improvement of Li-Rich Layered Cathode Material $Li[Li_{0.2}Mn_{0.54}Ni_{0.13}Co_{0.13}]O_2$ by ZrO_2 Coating. *Surf. Coat. Technol.* **2013**, *235*, 570−576.
(35) Li, G. R.; Feng, X.; Ding, Y.; Ye, S. H.; Gao, X. P. AlF_3-Coated $Li(Li_{0.17}Ni_{0.25}Mn_{0.58})O_2$ as Cathode Material for Li-Ion Batteries. *Electrochim. Acta* **2012**, *78*, 308−315.
(36) Liu, X. Y.; Liu, J. L.; Huang, T.; Yu, A. S. CaF_2-Coated $Li_{1.2}Mn_{0.54}Ni_{0.13}Co_{0.13}O_2$ as Cathode Materials for Li-Ion Batteries. *Electrochim. Acta* **2013**, *109*, 52−58.
(37) Cho, D. H.; Yashiro, H.; Sun, Y. K.; Myung, S. T. Electrochemical Properties of Polyaniline-Coated Li-Rich Nickel Manganese Oxide and Role of Polyaniline Coating Layer. *J. Electrochem. Soc.* **2014**, *161*, A142−A148.
(38) Kim, I. T.; Knight, J. C.; Celio, H.; Manthiram, A. Enhanced Electrochemical Performances of Li-Rich Layered Oxides by Surface Modification with Reduced Graphene Oxide/$AlPO_4$ Hybrid Coating. *J. Mater. Chem. A* **2014**, *2*, 8696−8704.
(39) Choi, N.-S.; Han, J. G.; Ha, S. Y.; Park, I.; Back, C. K. Recent Advances in the Electrolytes for Interfacial Stability of High-Voltage Cathodes in Lithium-Ion Batteries. *RSC Adv.* **2015**, *5*, 2732−2748.
(40) Lee, S. J.; Han, J. G.; Park, I.; Song, J.; Cho, J.; Kim, J. S.; Choi, N.-S. Effect of Lithium Bis(oxalato)borate Additive on Electrochemical Performance of $Li_{1.17}Ni_{0.17}Mn_{0.5}Co_{0.17}O_2$ Cathodes for Lithium-Ion Batteries. *J. Electrochem. Soc.* **2014**, *161*, A2012−A2019.
(41) Chernyshov, D. V.; Krachkovskiy, S. A.; Kapylou, A. V.; Bolshakov, I. A.; Shin, W. C.; Ue, M. Substituted Dioxaphosphinane as an Electrolyte Additive for High Voltage Lithium-Ion Cells with Overlithiated Layered Oxide. *J. Electrochem. Soc.* **2014**, *161*, A633−A642.
(42) Lee, D. J.; Im, D.; Ryu, Y. G.; Lee, S.; Yoon, J.; Lee, J.; Choi, W.; Jung, I.; Lee, S.; Doo, S. G. Phosphorus Derivatives as Electrolyte Additives for Lithium-Ion Battery: The Removal of O_2 Generated from Lithium-Rich Layered Oxide Cathode. *J. Power Sources* **2013**, *243*, 831−835.
(43) Li, Z. D.; Zhang, Y. C.; Xiang, H. F.; Ma, X. H.; Yuan, Q. F.; Wang, Q. S.; Chen, C. H. Trimethyl Phosphite as an Electrolyte Additive for High-Voltage Lithium-Ion Batteries Using Lithium-Rich Layered Oxide Cathode. *J. Power Sources* **2013**, *240*, 471−475.
(44) Song, Y. M.; Han, J. G.; Park, S.; Lee, K. T.; Choi, N.-S. A Multifunctional Phosphite-Containing Electrolyte for 5 V-Class $LiNi_{0.5}Mn_{1.5}O_4$ Cathodes with Superior Electrochemical Performance. *J. Mater. Chem. A* **2014**, *2*, 9506−9513.
(45) Yang, C.; Zhang, Q.; Ding, W.; Zang, J.; Lei, M.; Zheng, M.; Dong, Q. Improving the Electrochemical Performance of Layered Lithium-Rich Cathode Materials by Fabricating a Spinel Outer Layer with Ni^{3+}. *J. Mater. Chem. A* **2015**, *3*, 7554−7559.
(46) Song, B. H.; Liu, Z. W.; Lai, M. O.; Lu, L. Structural Evolution and the Capacity Fade Mechanism upon Long-Term Cycling in Li-Rich Cathode Material. *Phys. Chem. Chem. Phys.* **2012**, *14*, 12875−12883.
(47) Grosvenor, A. P.; Biesinger, M. C.; Smart, R. S. C.; Mclntyre, N. S. New Interpretations of XPS Spectra of Nickel Metal and Oxides. *Surf. Sci.* **2006**, *600*, 1771−1779.
(48) Shi, Y. L.; Shen, M. F.; Xu, S. D.; Qiu, X. Y.; Jiang, L.; Qiang, Y. H.; Zhuang, Q. C.; Sun, S. G. Electrochemical Impedance Spectroscopic Study of the Electronic and Ionic Transport Properties of NiF_2/C Composites. *Int. J. Electrochem. Sci.* **2011**, *6*, 3399−3415.
(49) Gaarenstroom, S. W.; Winograd, N. Initial and Final-State Effects in Esca Spectra of Cadmium and Silver-Oxides. *J. Chem. Phys.* **1977**, *67*, 3500−3506.
(50) Deshpande, R. D.; Ridgway, P.; Fu, Y.; Zhang, W.; Cai, J.; Battaglia, V. The Limited Effect of VC in Graphite/NMC Cells. *J. Electrochem. Soc.* **2015**, *162*, A330−A338.
(51) Cho, I. H.; Kim, S. S.; Shin, S. C.; Choi, N.-S. Effect of SEI on Capacity Losses of Spinel Lithium Manganese Oxide/Graphite Batteries Stored at 60 °C. *Electrochem. Solid-State Lett.* **2010**, *13*, A168−A172.
(52) Xia, Y. Y.; Zhou, Y. H.; Yoshio, M. Capacity Fading on Cycling of 4 V Li/$LiMn_2O_4$ Cells. *J. Electrochem. Soc.* **1997**, *144*, 2593−2600.
(53) Choi, N.-S.; Yeon, J. T.; Lee, Y. W.; Han, J. G.; Lee, K. T.; Kim, S. S. Degradation of Spinel Lithium Manganese Oxides by Low Oxidation Durability of $LiPF_6$-Based Electrolyte at 60 °C. *Solid State Ionics* **2012**, *219*, 41−48.
(54) Carroll, K. J.; Qian, D.; Fell, C.; Calvin, S.; Veith, G. M.; Chi, M. F.; Baggetto, L.; Meng, Y. S. Probing the Electrode/Electrolyte Interface in the Lithium Excess Layered Oxide $Li_{1.2}Ni_{0.2}Mn_{0.6}O_2$. *Phys. Chem. Chem. Phys.* **2013**, *15*, 11128−11138.
(55) Koga, H.; Croguennec, L.; Menetrier, M.; Mannessiez, P.; Weill, F.; Delmas, C. Different Oxygen Redox Participation for Bulk and Surface: A Possible Global Explanation for the Cycling Mechanism of $Li_{1.20}Mn_{0.54}Co_{0.13}Ni_{0.13}O_2$. *J. Power Sources* **2013**, *236*, 250−258.

DOI: 10.1021/acsami.5b01770
ACS Appl. Mater. Interfaces 2015, 7, 8319−8329